Applied Surface Science 473 (2019) 511–515

Contents lists available at ScienceDirect

Applied Surface Science

journal homepage: www.elsevier.com/locate/apsusc

Full Length Article

Surface effect of platinum catalyst-decorated mesoporous carbon support using the dissolution of zinc oxide for methanol oxidation

Geon-Hyoung An[a,1], Hyun-Gi Jo[b,1], Hyo-Jin Ahn[a,b,*]

[a] Program of Materials Science & Engineering, Convergence Institute of Biomedical Engineering and Biomaterials, Seoul 139-743, Republic of Korea
[b] Department of Materials Science and Engineering, Seoul National University of Science and Technology, Seoul 139-743, Republic of Korea

ARTICLE INFO

Keywords:
Direct methanol fuel cells
Support
Catalysts
Mesoporous
Carbon
Platinum nanocatalyst

ABSTRACT

Due to their excellent chemical stability, as well as low operating temperature, high energy density, and environment-friendliness, carbon supports are a prospective candidate for platinum (Pt) nanocatalysts in direct methanol fuel cells (DMFCs). However, numerous efforts to achieve the high efficiency for the energy conversion by carbon supports have faced considerable challenges owing to an inefficient utilization of the inside region, leading to the low electrochemical performance. Thus, in the present study, we propose an advanced surface technology for the mesoporous structure. The obtained Pt nanocatalyst-decorated mesoporous carbon nanofiber support offers a high anodic current density of 732 mA mg_{Pt}^{-1}, and an excellent catalytic stability as compared to the commercial Pt/C (20 wt% Pt on Vulcan carbon, De Nora S.P.A.) and Pt/CNF. Due to these characteristics, this advanced carbon support provides several, benefits such as the well-dispersed Pt nanocatalysts on the surface, as well as achieves a superb catalytic stability. In sum, the advanced carbon support is a promising candidate to improve the electrochemical performance of DMFCs.

1. Introduction

Renewable energy devices are of a key significance in terms of solving the foreseeable energy depletion problem and the global climate change. The fuel cells have been reported to have a large potential to convert the chemical energy into electricity. Among the various types of fuel cells, the typical low-temperature fuels as direct methanol fuel cells (DMFCs) are a promising renewable energy source due to their high energy density, low operating temperature, low emission of pollutants, and high energy conversion [1–3]. The DMFC consists of an anode, a cathode, an electrolyte, and a membrane. The methanol oxidation reaction (MOR) on the anode is one of the key elements needed for energy conversion performance in DMFCs [1–3]. However, there are three obstacles to an effective application of MOR in DMFCs, namely: (1) the high cost of Pt; (2) penchant to agglomerate of Pt; (3) poor CO tolerance. Therefore, Pt nanocatalysts need to be characterized by a high dispersion onto a support to acquire numerous electroactive sites between the methanol fuel and nanocatalyst surface, which can lead to an improved MOR [4–7]. Thus far, owing to their superb chemical properties and relative stability during MOR, carbon supports have been widely investigated for the efficient use of Pt nanocatalysts [4–7]. However, to further develop the DMFC technologies, an advanced carbon support is urgently needed so as to enhance the electrochemical performance.

In this context, numerous studies have sought to enhance the electrochemical performance of carbon supports. Among the proposed strategies, producing an advanced carbon support with a high surface area and mesoporous structure is a useful technique to achieve a good dispersion of Pt nanocatalysts on the surface, which can increase the electroactive sites [8–15]. Nevertheless, the inefficient use of the inside region for carbon supports still remains a problem and underlies the limited energy conversion performance.

In the present study, we propose an advanced surface technology of producing carbon supports using the mesoporous structure. The synthesis of mesoporous structure for carbon supports using dissolution of zinc oxide, which could be useful in improved electrochemical performance, has not yet been studied. Our results demonstrate that the Pt nanocatalyst-decorated mesoporous carbon nanofiber supports can be successfully fabricated using the electrospinning and impregnation methods. Moreover, the interlinked structure consisting of one-dimensional nanofibers as carbon nanofibers ensure a good dispersion of Pt nanocatalysts.

* Corresponding author at: Department of Materials Science and Engineering, Seoul National University of Science and Technology, Seoul 139-743, South Korea.
E-mail address: hjahn@seoultech.ac.kr (H.-J. Ahn).
[1] G.-H. An and H.-G. Jo contributed equally to this work.

https://doi.org/10.1016/j.apsusc.2018.12.175
Received 19 July 2018; Received in revised form 13 November 2018; Accepted 18 December 2018
Available online 19 December 2018
0169-4332/

2. Experimental

2.1. Synthesis of platinum catalyst-decorated mesoporous carbon nanofiber support (Pt/MPCNF)

The platinum catalyst-decorated mesoporous carbon nanofiber support (Pt/MPCNF) was successfully fabricated using the electrospinning and impregnation methods. For electrospinning, 10 wt% polyacrylonitrile (PAN, M_w = 150,000, Sigma-Aldrich, Germany) and 15 wt % zinc oxide (ZnO, nanopowder, 97% < 50 nm particle size, Sigma-Aldrich, Germany) were dissolved in N,N-Dimethylformamide (DMF, 99.8%, Sigma-Aldrich, Germany). The feed rate and voltage were retained at 0.05 mL h^{-1} and ~16 kV, respectively. To form the mesoporous structure, the as-spun nanofibers were stabilized at 230 °C for 3 h in air and then carbonized at 800 °C for 3 h under the nitrogen atmosphere. The carbonized nanofiber was calcined at 250 °C for 2 h under air to oxidize the Zn phases in the mesoporous carbon nanofibers to the ZnO phases. To decorate the Pt nanocatalysts on the support surface, the impregnation method was performed. The prepared support was dispersed in 0.28 mM $H_2PtCl_6{\cdot}xH_2O$ (≥99.9%, Sigma-Aldrich, Germany) solution and then reduced using the sodium borohydride solution (100 mg mL^{-1}, Sigma-Aldrich, Germany) to load 10 wt% Pt nanocatalysts on the support surface. To acquire the metallic Pt phases, the nanocatalysts were obtained using the freeze-dry process under −50 °C. For comparison, the carbon nanofibers (CNF) was synthesized without ZnO nanopowder. In addition, the platinum catalyst-decorated carbon nanofiber supports (Pt/CNF) were prepared under the same conditions, but without the ZnO nanoparticles.

2.2. Characterization

The structures and morphologies of the samples were inspected by field–emission scanning electron microscopy (SEM, Hitachi, SU8010) and transmission electron microscopy (TEM, Tecnai G^2, Gwangju Center, Korea Basic Science Institute). Energy-dispersive X-ray spectrometry mapping was performed to investigate the dispersion of elements in carbon nanofibers. The crystal structures and chemical bonding states were examined using X-ray diffractometry (XRD, Rigaku D/MAX-2500) and X-ray photoelectron spectroscopy (XPS, Thermo Electron, ESCALAB 250), respectively.

2.3. Electrochemical characterization

The methanol oxidation and catalytic stability were inspected using a potentiostat/galvanostat (Ecochemie Autolab, PGST302N) in three-electrode cells consisting of the working electrode (glassy carbon electrode, area = 0.0706 cm^2), the reference electrode (Ag/AgCl, sat. KCl) and the counter electrode (Pt gauze). To create the catalyst inks, Pt/MPCNF was dispersed in 2-propanol (99.5%, Sigma-Aldrich, Germany) with 20 wt% Nafion (Sigma-Aldrich, Germany) and then dropped on the working electrode. Thereafter, the electrochemical behavior was run using cyclic voltammograms (CV) in a 0.5 M H_2SO_4 and 2 M CH_3OH electrolyte (Sigma-Aldrich, Germany) at the scan rate of 50 mV s^{-1} between −0.2 and 1.0 V (vs. Ag/AgCl). To further explore the catalytic stability, chrono amperometry (CA) was performed in an electrolyte for 2000 s at the constant potential of 0.5 V. For comparison, the Pt/CNF and the commercial Pt/C were also prepared under the same conditions.

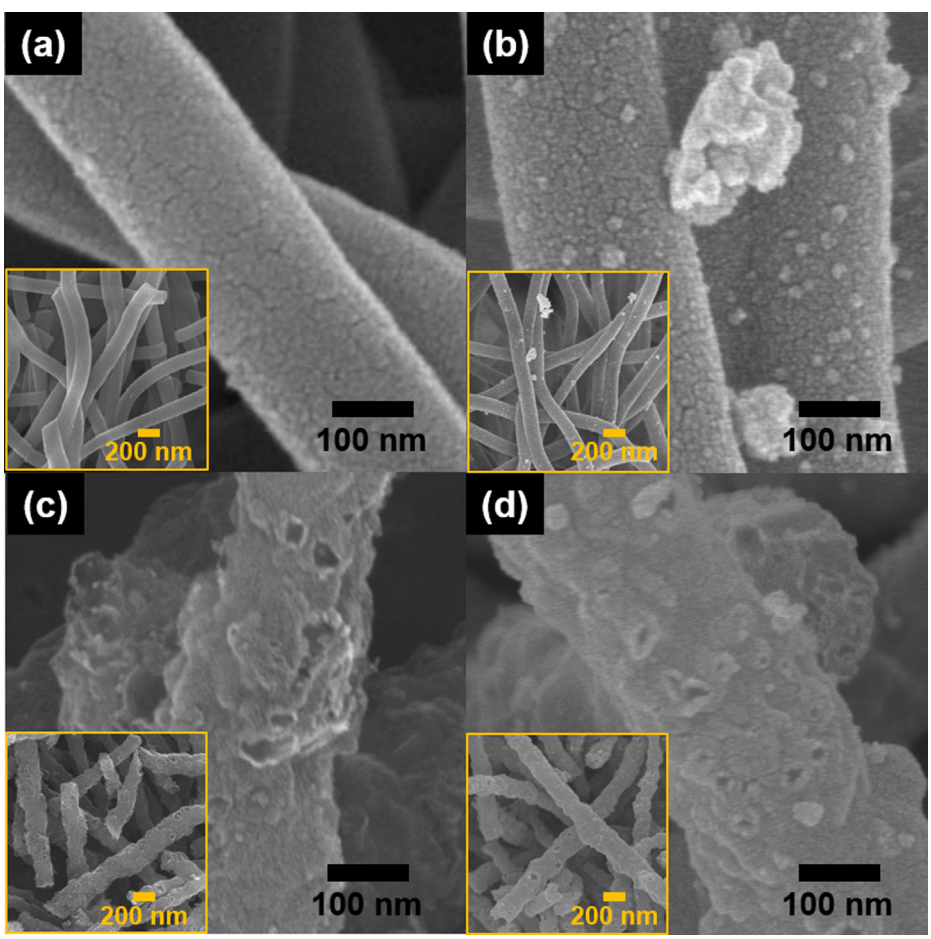

Fig. 1. SEM images of (a) the CNF support, (b) Pt/CNF, (c) the mesoporous CNF support, and (d) Pt/MPCNF.

3. Results and discussion

Fig. 1 shows the SEM images of the CNF support, Pt/CNF, mesoporous CNF support, and Pt/MPCNF. All catalysts showed an interlinked structure consisting of the one-dimensional nanofiber with the diameter of 211–236 nm, which can provide the favorable ionic diffusion electron transfer during the MOR. The CNF support (Fig. 1a) displayed a flat surface, implying an inefficient use of the inside region. The CNF support had the low surface area of 359 $m^2 g^{-1}$ and the low mesopore volume fraction of 15.3% (data not shown). After the application of the impregnation method, Pt/CNF (Fig. 1b) exhibited the agglomerated Pt nanocatalysts on the surface due to the low surface area of supports, leading to a poor electrochemical performance during MOR. The mesoporous CNF support (Fig. 1c) showed a novel architecture of mesoporous structure with craters. The formation of mesoporous structure of the CNF support can be attributed to the dissolution of ZnO nanoparticles during the carbonization process. The ZnO nanoparticles in CNF were transferred to metallic Zn and then melted at the temperature over 419.5 °C [16]. Thereafter, the melted Zn was partly vaporized to generate the mesoporous structure [16]. The mesoporous CNF support had the high surface area of 651 $m^2 g^{-1}$ and the high mesopore volume fraction of 80.3% (data not shown). Furthermore, Pt/MPCNF (Fig. 1d) exhibited a novel architecture of the mesoporous structure without the agglomerated Pt nanocatalysts on the surface, indicating that the inefficient use of the inside region of carbon supports with a high surface area and a high mesopore volume fraction could be the sufficient area for the decoration of Pt nanocatalysts on the supports. To determine the morphological properties of the supports and catalysts, TEM measurement was performed.

Fig. 2 shows low-magnification (Fig. 2a–d) and high-magnification (Fig. 2e–h) TEM images of the CNF support, Pt/CNF, mesoporous CNF support, and Pt/MPCNF. The CNF support (Fig. 2a and e) presented a uniform contrast, implying the only carbon phase without a porous structure. On the other hand, the dark spots of Pt/CNF (Fig. 2b and f) are the decorated Pt nanocatalysts on the surface. Unfortunately, Pt/CNF showed the agglomerated Pt nanocatalysts of 21–42 nm in size. The large size of Pt nanocatalysts is ineffective for MOR. Therefore, the advanced CNF support with a high surface area and a high mesopore volume fraction is essential to improve MOR. Interestingly, the mesoporous CNF support (Fig. 2c and g) displayed the two types of contrast, implying the mesopores of CNF support and ZnO nanoparticles (2–10 nm) by a dissolution of the ZnO nanoparticles during the carbonization. The embedded ZnO nanoparticles in the mesoporous CNF support can inhibit CO poisoning of catalysts using the oxidizing adsorbed CO to CO_2, leading the enhanced MOR. Of note, Pt/MPCNF (Fig. 2d and h) revealed well-dispersed Pt nanocatalysts without agglomeration, suggesting that a high surface area and a high mesopore volume fraction could supply the large sites for Pt nanocatalysts. In addition, Pt/MPCNF indicated the nanosized catalysts (3–5 nm) and clear lattice fringes with the spacing of 0.22 nm corresponding to the (1 1 1) planes of face-centered cubic Pt phases [17]. Pt nanocatalysts were penetrated through the pores inside. This was confirmed by TEM results (Fig. S1). To inspect the distribution of C, Zn, and Pt, the TEM–EDS mapping analysis was performed (Fig. 2i). The EDS results, which revealed that well-dispersed ZnO and Pt are embedded in the mesoporous CNF support, demonstrate that C, Zn, O, and Pt atoms are well dispersed.

Supplementary data associated with this article can be found, in the online version, at https://doi.org/10.1016/j.apsusc.2018.12.175.

Fig. 3a shows the XRD pattern (see Fig. 3a) of the CNF support, Pt/CNF, mesoporous CNF support; Pt/MPCNF was conducted to investigate their crystal structure. The main diffraction peak of the CNF

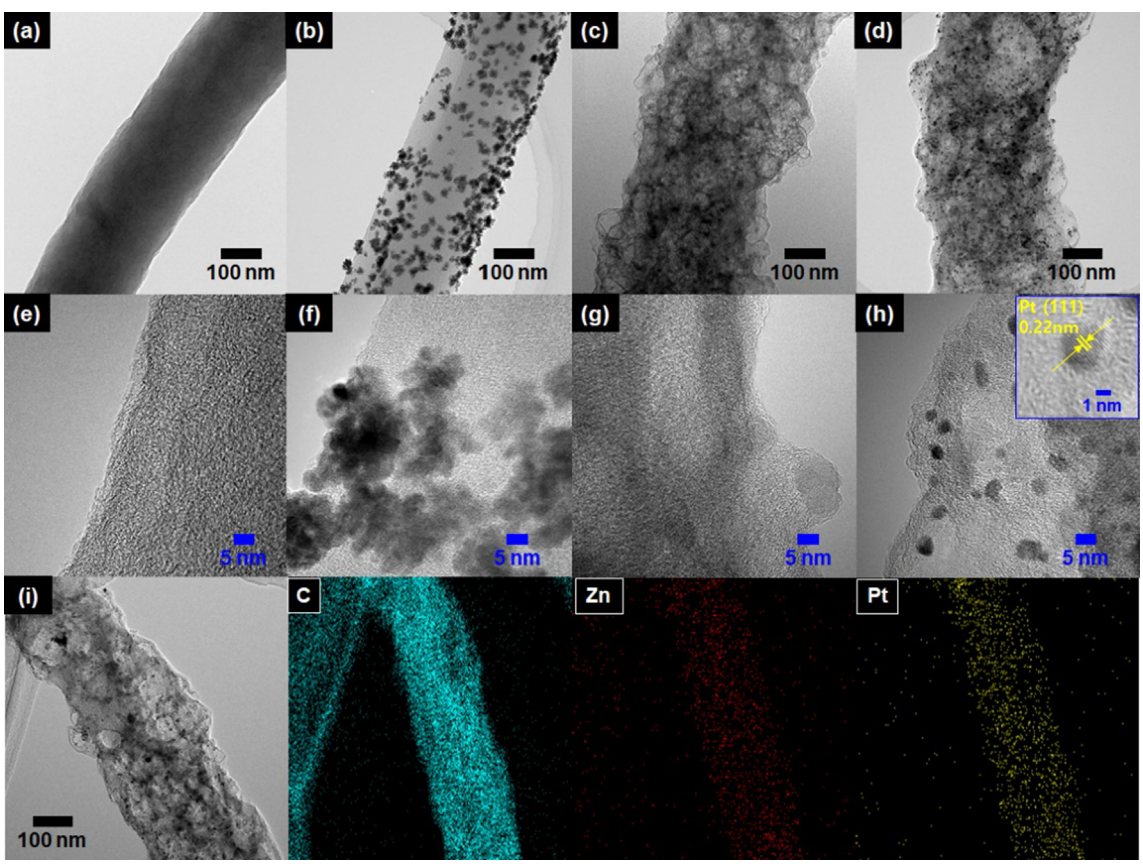

Fig. 2. (a–d) Low-resolution and (e–h) high-resolution TEM images of the CNF support, Pt/CNF, mesoporous CNF support, and Pt/MPCNF. (i) TEM-EDS mapping data of Pt/MPCNF.

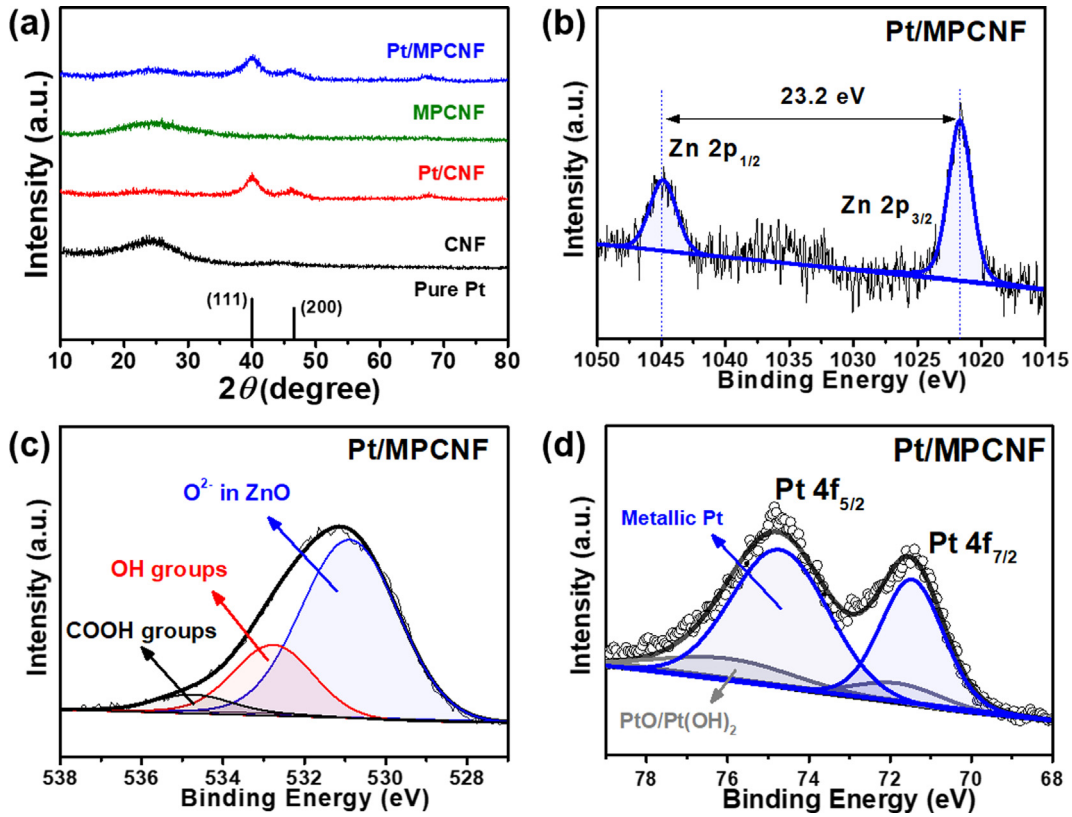

Fig. 3. (a) XRD patterns of the CNF support, Pt/CNF, mesoporous CNF support, and Pt/MPCNF. (b) Zn 2p, (c) O 1s, and (d) Pt 4f of Pt/MPCNF.

support and mesoporous CNF support was observed at 25.0°, corresponding to the (0 0 2) plane of graphite layers [18,19]. On the other hand, Pt/CNF and Pt/MPCNF indicated the main diffraction peaks at 39.7° and 46.2°, respectively, corresponding to the (1 1 1) and (2 0 0) planes of Pt phases (face-centered structure, space group *Fm3m* [2 2 5], JCPDS, 04-0802). To prove the chemical bonding features of Pt/MPCNF, the XPS measurements were performed. The spectral peaks were standardized by C 1s line (284.5 eV). The Zn 2p XPS spectral peaks of Pt/MPCNF (see Fig. 3b) showed two signals at ~1022.0 eV and ~1045.1 eV with the spin energy separation of 23.2 eV, which corresponded to the Zn $2p_{3/2}$ and Zn $2p_{1/2}$ of ZnO phase, respectively [16,20]. The deconvolution of the O 1s XPS spectral peaks of Pt/MPCNF is shown in Fig. 3c. The lower energy peak at 531.0 eV was attributed to the typical value of O_2^- in ZnO. The intermediate energy peak at 532.6 eV was associated with the OH groups. Finally, the higher energy peak at 533.7 eV was related to the COOH groups [16]. These results indicate the formation of ZnO phases of Pt/MPCNF, which can inhibit CO poisoning of catalysts using oxidizing adsorbed CO to CO_2 during the MOR. Fig. 3d shows the Pt 4f XPS spectral peaks of Pt/MPCNF at 71.4 eV and 74.8 eV corresponding to the metallic Pt phase [21].

To further explore the MOR performance of Pt/CNF and Pt/MPCNF, the CV measurement was implemented in the voltage range of −0.2 and 1.0 V in a 0.5 M H_2SO_4 and 2 M CH_3OH electrolyte at 50 mV s^{-1} (see Fig. 4a). To normalize the measured data, the mass of Pt loading (8 mg cm^{-2}) was used. As is well known, the MOR turns out 6 electrons, 6 protons, and carbon dioxide ($CH_3OH + H_2O \rightarrow 6e^- + 6H^+ + CO_2$) [1–3,5]. For comparison, the commercial Pt/C was prepared under the same conditions. CV curves appeared to have typical MOR peaks, including the intermediate species such as CO, COOH, and CHO in the backward scan and the methanol oxidation peak in the forward scan [4–7,12–15]. Therefore, the value of anodic current density related to the methanol oxidation peak in the forward scan is a significant index [4–7,12–18]. The maximum anodic current densities of the commercial Pt/C, Pt/CNF, and Pt/MPCNF were 495, 383, and 732 mA mg_{Pt}^{-1},

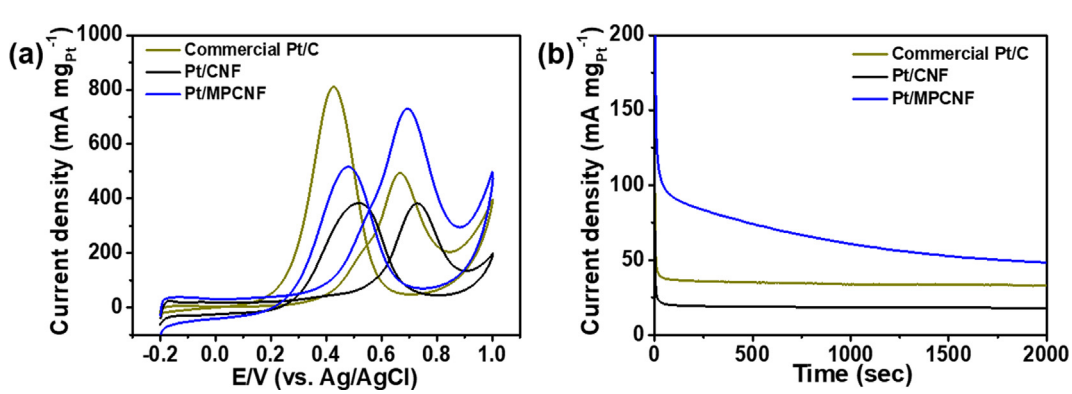

Fig. 4. (a) Cyclic voltammetry (CV) measurements of methanol oxidation of commercial Pt/C, Pt/CNF, and Pt/MPCNF at the scan rate of 50 mV s^{-1} in the voltage range of −0.2 to 1.0 V. (b) Chronoamperometry (CA) of the commercial Pt/C, Pt/CNF, and Pt/MPCNF in 0.5 M H_2SO_4 and 2 M CH_3OH electrolyte at 0.5 V.

respectively. A higher anodic current density of Pt/MPCNF entails a higher number of electrons as compared to other catalysts, implying an improved electrochemical performance of MOR. These results can mainly be ascribed to the well-dispersed Pt nanocatalysts related to the numerous electroactive sites during the MOR. In addition, it is widely known that Pt nanocatalysts tend to the intermediate species on the Pt surfaces, resulting in a higher ratio of the forward peak current (I_F) to the backward peak current (I_B). The I_F/I_B ratio of Pt/MPCNF is the highest (1.4) as compared to the commercial Pt/C (0.6) and Pt/CNF (1.0), implying the excellent CO tolerance during MOR. The enhanced CO tolerance can be defined by the bifunctional effect ($Zn–OH + Pt–CO \rightarrow Pt + Zn + CO_2 + H^+ + e^-$) [22,23]. Thus, the existence of the ZnO phase of Pt/MPCNF facilitates removing the adsorbed CO species using the abundant adsorbed hydroxyl species, resulting in clean electroactive sites of Pt nanocatalysts. One of the significant issues for the DMFC technology is the catalytic stability. Therefore, to inspect catalytic stability of catalysts, chrono amperometry (CA) was carried out at 0.5 V in a 0.5 M H_2SO_4 and 2 M CH_3OH electrolyte for 2000 s (see Fig. 4b). The decay of current density was monitored owing to the adsorption of SO_4^{2-} anions and intermediate species onto the Pt surface. Despite the disturbance of absorption for anion and intermediate species, Pt/MPCNF indicated the lowest deterioration rate and highest current density. These results suggest that ZnO phases could enhance the catalytic stability due to the bifunctional effect.

The enhanced electrochemical performance of Pt/MPCNF was achieved due to two major factors. First, the good distribution of Pt nanocatalyst afforded numerous electroactive sites between the Pt nanocatalyst and the electrolyte, leading to an improved anodic current density during MOR. Second, the existence of the ZnO phases in Pt/MPCNF made it possible to resist the adsorbed CO species using the abundant adsorbed hydroxyl species during MOR, which resulted in an enhanced catalytic stability.

4. Conclusions

In the present study, Pt/MPCNF as a catalyst for MOR was fabricated using the electrospinning and impregnation methods. The Pt/MPCNF showed a good dispersion of Pt nanocatalysts (3–5 nm) without the agglomeration, meaning that the inefficient use of the inside region for the CNF supports using the high surface area and the high mesopore volume fraction could serve the sufficient area for the decoration of Pt nanocatalysts on the supports. Pt/MPCNF showed an improved electrochemical behavior with the highest anodic current density of 732 mA mg_{Pt}^{-1}, and an excellent catalytic stability compared to commercial Pt/C and Pt/CNF. The superb electrochemical performance of Pt/MPCNF can be attributed to the following two main factors: (I) the enhanced anodic current density related to the good distribution of Pt electrocatalyst; (II) the excellent catalytic stability related to the existence of the ZnO phases. In sum, Pt/MPCNF could be a promising candidate to replace the commercial Pt/C for application in DMFCs.

Acknowledgments

This study was supported by Grant No. 10047747 from Ministry of Trade, Industry, And Energy (MOTIE) and Fundamental R&D Program for Strategic Core Technology of Materials funded by the Ministry of Trade, Industry, and Energy, Republic of Korea.

References

[1] X. Shan, I.D. Perez, L. Wang, P. Wiktor, Y. Gu, L. Zhang, W. Wang, J. Lu, S. Wang, Q. Gong, J. Li, N. Tao, Imaging the electrocatalytic activity of single nanoparticles, Nat. Nanotechnol. 7 (2012) 668–672.
[2] M.K. Debe, Electrocatalyst approaches and challenges for automotive fuel cells, Nature 486 (2012) 43–51.
[3] B.C.H. Steele, A. Heinzel, Materials for fuel-cell technologies, Nature 414 (2001) 345–352.
[4] Y.S. Kang, N. Jung, K.H. Choi, M.J. Lee, M. Ahn, Y.H. Cho, Y.E. Sung, Anode electrode with carbon buffer layer for improving methanol oxidation reaction in direct methanol fuel cell, Appl. Surf. Sci. 290 (2014) 246–251.
[5] G.H. An, E.H. Lee, H.J. Ahn, Ruthenium and ruthenium oxide nanofiber supports for enhanced activity of platinum electrocatalysts in the methanol oxidation reaction, Phys. Chem. Chem. Phys. 18 (2016) 14859–14866.
[6] X. Li, L. Luo, F. Peng, H. Wang, H. Yu, Enhanced activity of Pt/CNTs anode catalyst for direct methanol fuel cells using Ni2P as co-catalyst, Appl. Surf. Sci. 434 (2018) 534–539.
[7] G.H. An, H.J. Ahn, Pt electrocatalyst-loaded carbon nanofibre–Ru core–shell supports for improved methanol electrooxidation, J. Electroanal. Chem. 707 (2013) 74–77.
[8] N. Kakati, J. Maiti, S.H. Lee, B. Viswanathan, Y.S. Yoon, Anode catalysts for direct methanol fuel cells in acidic media: do we have any alternative for Pt or Pt–Ru, Chem. Rev. 114 (2014) 12397–12429.
[9] X. Li, A. Faghri, Review and advances of direct methanol fuel cells (DMFCs) part I: Design, fabrication, and testing with high concentration methanol solutions, J. Power Sources 226 (2013) 223–240.
[10] H. Liu, C. Song, L. Zhang, J. Zhang, H. Wang, D.P. Wilkinson, A review of anode catalysis in the direct methanol fuel cell, J. Power Sources 155 (2006) 95–110.
[11] G. Zhao, J. He, C. Zhang, J. Zhou, X. Chen, T. Wang, Highly dispersed Pt nanoparticles on mesoporous carbon nanofibers prepared by two templates, J. Phys. Chem. C 112 (2008) 1028–1033.
[12] Z. Wen, J. Liu, J. Li, Core/shell Pt/C nanoparticles embedded in mesoporous carbon as a methanol-tolerant cathode catalyst in direct methanol fuel Cells, Adv. Mater. 20 (2008) 743–747.
[13] H. Zhang, C. Cheng, ALD of Pt nanotube arrays supported on a carbon fiber cloth as a high-performance electrocatalyst for methanol oxidation, J. Mater. Chem. A 4 (2016) 15961–15967.
[14] J.R.C. Salgado, F. Alcaide, G. Álvarez, L. Calvillo, M.J. Lázaro, E. Pastor, Pt–Ru electrocatalysts supported on ordered mesoporous carbon for direct methanol fuel cell, J. Power Sources 195 (2010) 4022–4029.
[15] C.-D. Dong, C.-W. Chen, C.-F. Chen, C.-M. Hung, Platinum particles supported on mesoporous carbons: fabrication and electrocatalytic performance in methanol-tolerant oxygen-reduction reactions, Sci. Rep. 4 (2014) 5790.
[16] G.H. An, D.Y. Lee, H.J. Ahn, Tunneled mesoporous carbon nanofibers with embedded ZnO nanoparticles for ultrafast lithium storage, ACS Appl. Mater. Interf. 9 (2017) 12478–12485.
[17] G.H. An, H.G. Jo, H.J. Ahn, Platinum nanoparticles on nitrogen-doped carbon and nickel composites surfaces: a high electrical conductivity for methanol oxidation reaction, J. Alloys Compd. 763 (2018) 250–256.
[18] G.H. An, D.Y. Lee, H.J. Ahn, Vanadium nitride encapsulated carbon fibre networks with furrowed porous surfaces for ultrafast asymmetric supercapacitors with robust cycle life, J. Mater. Chem. A 5 (2017) 19714–19720.
[19] G.H. An, H. Kim, H.J. Ahn, Improved ionic diffusion through the mesoporous carbon skin on silicon nanoparticles embedded in carbon for ultrafast lithium storage, ACS Appl. Mater. Interf. 10 (2018) 6235–6244.
[20] G.-H. An, S.N. Cha, J.I. Sohn, Surface tailoring of zinc electrodes for energy storage devices with high energy densities and long cycle life, Appl. Surf. Sci. 467–468 (2019) 1157–1160.
[21] G.H. An, H.J. Ahn, W.K. Hong, Electrochemical properties for high surface area and improved electrical conductivity of platinum-embedded porous carbon nanofibers, J. Power Sources 274 (2015) 536–541.
[22] H. Ahouari, A. Soualah, A.L. Valant, L. Pinard, Y. Pouilloux, Hydrogenation of CO_2 into hydrocarbons over bifunctional system Cu–ZnO/Al_2O_3 + HZSM-5: effect of proximity between the acidic and methanol synthesis sites, Cr. Chim. 18 (2015) 1264–1269.
[23] S. Baier, C.D. Damsgaard, M. Klumpp, J. Reinhardt, T. Sheppard, Z. Balogh, T. Kasama, F. Benzi, J.B. Wagner, W. Schwieger, C.G. Schroer, J.D. Grunwaldt, Stability of a bifunctional Cu-based core@zeolite shell catalyst for dimethyl ether synthesis under redox conditions studied by environmental transmission electron microscopy and in situ X-ray ptychography, Microsc. Microanal. 23 (2017) 501–512.